Medical Engineering and Physics 000 (2017) 1–7

Contents lists available at ScienceDirect

Medical Engineering and Physics

journal homepage: www.elsevier.com/locate/medengphy

Technical note

Iterative approach for 3D reconstruction of the femur from un-calibrated 2D radiographic images

Kibeom Youn[a], Moon Seok Park[b], Jehee Lee[a,*]

[a] School of Computer Science and Engineering, Seoul National University, 1 Kwanak-Ro, Kwanak-Gu, Seoul 151-744, Republic of Korea
[b] Department of Orthopedic Surgery, Seoul National University Bundang Hospital, 300 Gumi-Dong, Bundang-Gu, Sungnam, Kyungki 463-707, Republic of Korea

ARTICLE INFO

Article history:
Received 7 April 2017
Revised 26 July 2017
Accepted 27 August 2017
Available online xxx

Keywords:
Cerebral palsy
Femur
Bony deformities
X-ray
Computed tomography
3D reconstruction
Self-calibration
Statistical shape model

ABSTRACT

Three-dimensional reconstruction of the femur is important for surgical planning in patients with cerebral palsy. This study aimed to reconstruct the three-dimensional femur shape from un-calibrated bi-planar radiographic images using self-calibration to allow for low-dose preoperative planning. The existing self-calibration techniques require anatomical landmarks that are clearly visible on bi-planar images, which are not available on the femur. In our newly developed method, the self-calibration is performed so that the contour of the statistical shape matches the image contour while the statistical shape is concomitantly optimized. The proposed approach uses conventional radiograph systems and can be easily incorporated into existing clinical protocols, as compared to other reconstruction methods.

1. Introduction

Cerebral palsy (CP) is a group of permanent developmental disorders caused by non-progressive disturbances occurring in the immature brain of a developing fetus or infant. Increased femoral anteversion and coxa valga are common proximal femoral conditions in patients with CP. Clinicians often use three-dimensional (3D) reconstructed computed tomography (CT) images to accurately measure the femoral anteversion when planning femoral derotation osteotomy [1,2]. However, the high radiation dose of CT remains a concern, especially for children, who are more vulnerable to radiation compared to adults.

As an alternative to CT, the EOS® system [3] has been proposed to reconstruct 3D bony shapes from calibrated bi-planar X-ray images as a means to reduce the radiation exposure [4–6]. The camera alignment in EOS® is predetermined; thus, it acquires two orthogonal head-to-feet calibrated radiographic images. However, this system requires another apparatus in addition to the conventional radiographic system, and the cost for the device installation is high and the space occupied is substantial. Other existing methods use conventional radiographic systems but require a rigid calibration object such as a metal marker to obtain clearly visible stereo points on the radiographs [7–14]. However, positioning the calibration object is often cumbersome and inconvenient, because it disturbs the existing clinical routines. Thus, studies using anatomical landmarks as an alternative calibration object have been increasingly conducted. This kind of approach is called 'self-calibration' and has been shown to be successful with spinal reconstruction, in which the bony shapes of the vertebrae provide a rich set of anatomical landmarks [15,16]. However, for the femur, the use of self-calibration is challenging, owing to the ambiguous landmarks. In the present study, we hypothesized that the contour of the femur on images can be used for the calibration instead of metal markers or anatomical landmarks.

Accordingly, the purposes of this study were: 1) to develop a new 3D reconstruction method of the femur from un-calibrated bi-planar radiographic images, which uses the conventional radiographic systems and does not require any calibration object; and 2) to validate this newly developed method.

2. Materials and methods

This study was approved by the institutional review board of Seoul National University Bundang Hospital (IRB No. B-1502/288-104) and the procedures followed were in accordance with the Helsinki Declaration of 1975, as revised in 2000. The need for

* Corresponding author.
E-mail addresses: pmsmed@gmail.com (M.S. Park), jehee@mrl.snu.ac.kr (J. Lee).

http://dx.doi.org/10.1016/j.medengphy.2017.08.016
1350-4533/

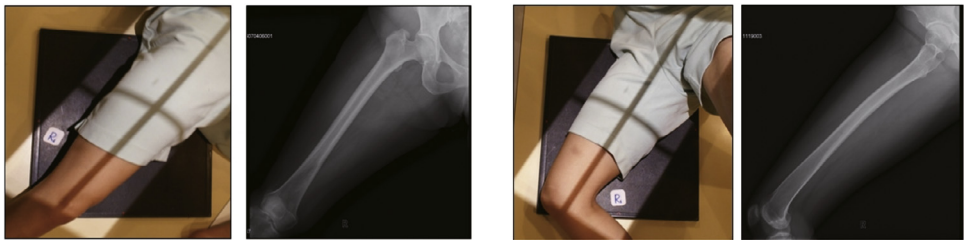

Fig. 1. Anterior–posterior (AP) and lateral (LAT) imaging protocols. In the LAT view, the pelvis is rotated slightly posteriorly to prevent overlap with the femur head.

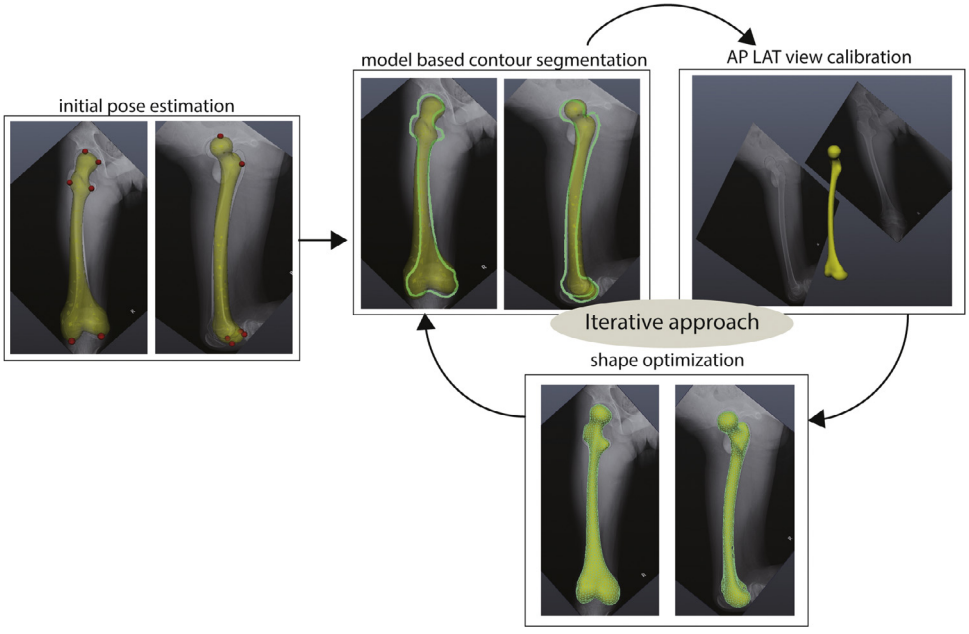

Fig 2. System overview: the anterior–posterior (AP) and lateral (LAT) views are initially pose-estimated using user inputted six points and its 3D correspondences. The image contour is segmented based on the projected contour of the 3D femur. The AP and LAT views are calibrated more accurately using contour correspondences. The shape is optimized so that it projected contour to match the segmented contour. These steps are iteratively performed until convergence.

informed consent was waived due to the retrospective nature of this study. A total of 80 patients with CP were enrolled. CT data of 54 children were used for constructing the statistical shape model (SSM). CT data of two children were used for the generation of 37 digitally reconstructed radiographs (DRRs) to test the calibration error. Finally, anterior–posterior (AP) and lateral (LAT) radiographs and CT data of 24 children were used for the validation of shape reconstruction.

2.1. System overview

The input of our system comprises AP- and LAT-view radiographs, which are not necessarily orthogonal, that is, they are uncalibrated. Fig. 1 shows the patient posture in the supine position. For the LAT radiographs, the pelvis is rotated slightly to the back so that it does not overlap with the femur head. If the length of the femur is longer than the plate length, the shaft axis of the femur is positioned diagonally to the image plate; otherwise, it is aligned with the longitudinal axis.

The user chooses six points on each radiograph manually based on rough estimation. These inputs act as landmarks for the initial calibration and contour extraction. The overall process consists of the following steps (Fig. 2): 1) Initial pose estimation is performed using the mean of the SSM and the six user-inputted points. 2) Iteratively, the following steps are solved until convergence: a) the image contour is segmented based on the projected contour of the SSM, b) contour-based pose estimation between the SSM and radiographic images is performed, and c) the 3D shape is deformed to match the projected AP and LAT contours of the 3D shape in the given views with segmented contours from the images.

2.2. Statistical shape model

Our dataset and SSM come from the previous research of Park et al. [17]. The dataset consists of CT data of the femurs of 54 patients with CP. The femurs exhibit a wide variety of shape deformities, and the dataset thus covers a wide range of subject variance. The mean femoral anteversion angle was 35.1° and the standard deviation (SD) was 12.1°. They validated the SSM using leave-one-out cross test. Clinical measurements of CT image and reconstructed SSM showed high Intraclass Correlation Coefficient (ICC). The reconstructed shape models from CT were processed to have an identical structure and the same number of vertices using the algorithm proposed by Ferrarini et al. [18]. In this method, the shape correspondences were obtained by iteratively adapting the reference shape to the other shapes. The shape is represented as the sum of the mean and linear combination of the principle components with coefficients, using principal component analysis, as follows:

$$P_i = \left(M_i + \sum_{j=1}^{n} V_i[j] \cdot c_j \right) \quad (1)$$

where M_i is the position of the ith vertex of the mean shape; $V_i[j]$ is the three dimensional sub-rows of the jth principal component

Please cite this article as: K. Youn et al., Iterative approach for 3D reconstruction of the femur from un-calibrated 2D radiographic images, Medical Engineering and Physics (2017), http://dx.doi.org/10.1016/j.medengphy.2017.08.016

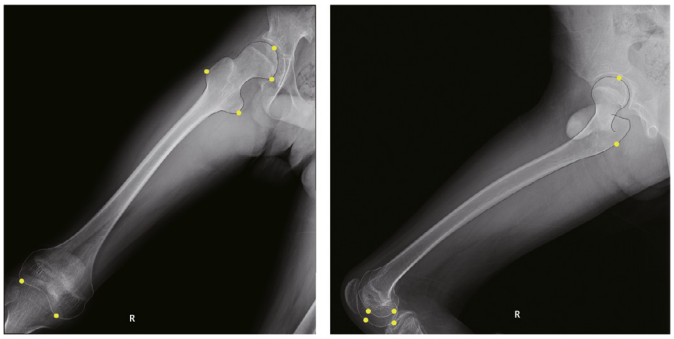

Fig. 3. a) In the AP view, the most proximal and medial points of the femur head, most lateral point of the greater trochanter and most medial point of the lesser trochanter, and most distal points of the condyles are selected along the shaft axis. b) In the LAT view, the most proximal point of the femur head, most lateral point of the greater trochanters, and most posterior and distal points of the condyles are selected along the shaft axis.

vector corresponding to the ith vertex of the mesh; and c_j is the coefficient of the jth principal component. The principal components are the shape offset vectors, which represent major variance in shape. The first principle component shows a close relation with the neck-shaft angle, and the second component relates with the femoral anteversion angle. The remaining components have mixed influence.

2.3. Initial pose estimation

The calibration starts from the orthogonal positions of the AP and LAT views as an initial guess. The pose estimation is solved by the Perspective-n-Point (PnP) method using six 2D–3D corresponding points [19]. The user inputs them to indicate the anatomical boundaries of the subject's femur (Fig. 3). The corresponding 3D points on the shape are searched from the vertices of the statistical shape.

2.4. Iterative approach

The contour segmentation, contour-based pose estimation, and statistical shape optimization are iteratively performed to refine the calibration and shape. The contour is segmented by selecting ordered points whose path is conformal to the contour of a 3D object in a given view. First, the image is canny-edge detected, and the detected points are Delaunay triangulated. The contour and surface normal vectors of the SSM are projected onto the image. The Delaunay triangulated edges form edges of a graph and their weights are given by the conformity to the projected contour of the SSM. Finally, the image contour is obtained by the graph shortest path algorithm.

$$W = W_N \times W_D$$
$$W_N = a + \frac{|0.5\pi - \angle(q_1 - q_2, n(p_1) + n(p_2))|}{b}, \quad W_D = d\|q_1 - q_2\| \tag{2}$$

where W is the weight of a graph edge between image points q_1 and q_2; n denotes a projected surface normal vector; p_1 and p_2 are a closest distance points of q_1 and q_2 respectively; and a, b, d are adjustable parameters depending on image quality. We set $a = 0.5, b = \frac{\pi}{6}, d = 1$ for our test set. The parameters were adjusted manually by observing the segmentation results of test set. In the AP view, all six points lie on the contour. In the LAT view, the two contours are segmented separately to distinguish overlapped contours (Fig. 4).

For the calibration, contour-based pose estimation is performed using the segmented image contour and the projected contour of the femur. The projected contour is also refined to have the same structure as the segmented 2D contour by means of the graph shortest path formulation, which is introduced at segmentation. The difference is that the projected 3D points are used instead of the edge-detected points of the image. Having obtained the contours of the 3D object and the image, we match the closest pairings from the projected 3D contour to the image contour. We used a KD-tree structure for the image contour pixels to query the closest point in order to reduce computation. The user-inputted six points and matched 3D points are given a high weight and joined with the contour matching pairs for pose-estimation. We used the PnP method iteratively to estimate the AP and LAT views using the above pairs [19]. Given the calibrated views, we optimized the statistical shape to fit with the segmented contours of the AP and LAT planes. The statistical shape parameters, that is, the coefficient of 10 principle components to minimize the sum of the projection error at the AP and LAT views, are optimized. Subsequently, the shape coefficient is updated from the current value to minimize the following error term:

$$\mathrm{E}(\mathrm{c}+\Delta\mathrm{c}) = \sum_{\mathrm{i}\in C} \left\| p_\mathrm{i} - (\mathrm{P}|_{zi} + \epsilon) \times \left[m_\mathrm{i} + \sum_{\mathrm{j}=1}^{10} \mathrm{V_i[j]} \cdot \left(\mathrm{c_j} + \Delta\mathrm{c_j}\right) \right] \right\|^2$$
$$\mathrm{E}(\mathrm{c}+\Delta\mathrm{c}) = \|\mathrm{A}\Delta\mathrm{c} + \mathrm{b}\|^2 + \epsilon$$
$$\text{where } \mathrm{A_i} = \mathrm{P}|_{zi}\mathrm{V_i}, \ \mathrm{b_i} = p_\mathrm{i} - \mathrm{P}|_{zi}\left(m_\mathrm{i} + \sum_{\mathrm{j}=1}^{10} \mathrm{V_i[j]} \cdot \mathrm{c_j}\right) \tag{3}$$

Here, the subscript i represents the sub-rows, which correspond to the ith vertex of the shape mesh; C is the index set of vertices which lie on the contour; $\mathrm{P}|_{zi}$ is the perspective projection matrix, which depends on the z coordinate of the vertex to be projected; p_i is the closest point of the segmented image contour; b_i is the difference vector between the image point and the projected vertex of the femur contour; and A_i is a matrix with projections of the principal components as columns. An incremental modification of c results in a small change of the projection matrix, which can be ignored. Given the projection matrix fixed, the delta of the shape coefficients is optimized by the least-square fitting method.

2.5. Validation

To validate our self-calibration method, we synthesized 37 biplanar imaging environments using digitally reconstructed radiographs extracted from the CT images of two patients with CP. The rotation of each plane from its orthogonal position was decomposed by Euler angles. We measured the element-wise difference between the ground-truth Euler angles and calibrated Euler angles. The test set covers a range of $\pm 35°$ variation in the Y axis and $> 0°$ in the X axis for the AP view. For the LAT view, ranges of $\pm 35°$ in both the Y and X axes were covered. An angle in the X axis of $> 0°$ means that the distal femur is heading forward relative to the proximal femur. In cases of angles $< 0°$ in the X axis, the AP views cannot identify distal femur shapes; thus, we excluded these cases. The Y axis corresponds to shaft axis of femur and the rotation of Y axis corresponds to the rotation of hip.

We first estimated the accuracy of the contour pose-estimation with prior shapes constructed from CT images using Mimics software [20] as a means to exclude shape-reconstruction error. The accuracy with these prior shapes indicates the maximum accuracy that can be achieved by our method. We excluded cases of translation errors, because translation is related to the absolute scale of a shape, which cannot be decided without a calibration object. Next,

Please cite this article as: K. Youn et al., Iterative approach for 3D reconstruction of the femur from un-calibrated 2D radiographic images, Medical Engineering and Physics (2017), http://dx.doi.org/10.1016/j.medengphy.2017.08.016

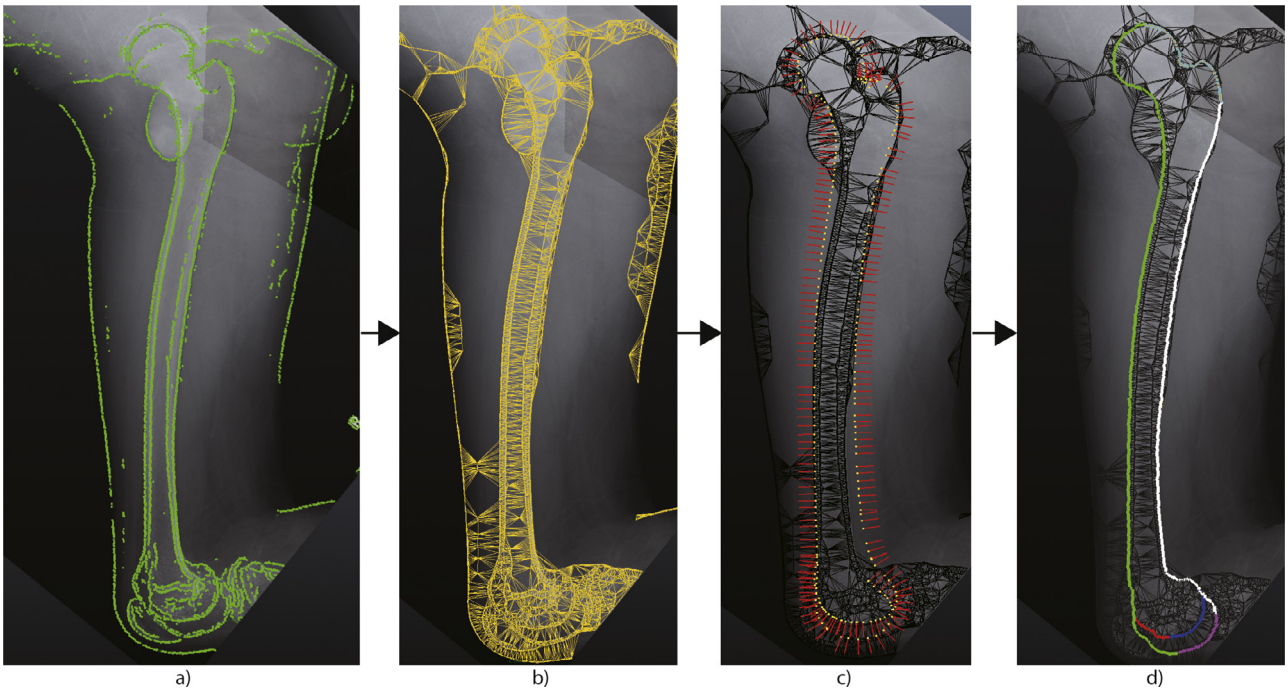

Fig. 4. Segmentation overview. a) Canny-edge detection. b) The canny-edge detected points are Delaunay triangulated to extract the possible path connections. c) The triangulated edge is given a weight of conformity according to how well the edge aligns with the projected contour of statistical shape model (SSM). d) The shortest path, in which the sum of the weight is minimized while passing through the manually inputted 6 points, is selected.

we estimated the accuracy of the contour pose-estimation with our SSM to show the effects of shape optimization on calibration.

To assess the shape reconstruction accuracy, we collected the AP and LAT radiographic images and CT data of 24 children with CP. Subsequently, we reconstructed 24 femurs using our method, and measured the distance from the vertex point of the SSM to the closest point on the ground-truth surface. The shape difference is presented as the Hausdorff distance and point-to-surface root mean squared (PS-RMS) between the ground-truth shape and optimized SSM. The SSM was scaled to have the same length as the ground-truth shape and was registered by iterative closest point algorithm for shape comparison.

2.6. Statistical method

For statistical independence, we used separate data sets for building the SSM and for testing the calibration and reconstruction errors. The calibration error was measured by the difference between the ground-truth angle of the DRR and the calibrated angles. The mean, standard deviation, 95% confidence interval (CI), and maximum value of the calibration error were used for validation. The reconstruction errors were measured by the Hausdorff distance and PS-RMS (in mm) between the optimized shape and ground-truth shape obtained from CT. The mean, standard deviation, 95% CI, and maximum values were used for validation.

3. Results

We used 37 bi-planar DRRs of CT of patients with CP for the validation of the calibration. The calibration errors with ground-truth vs. SSM were compared for each AP and LAT view (Table 1).

AP and LAT radiographic images and CT data of 24 children with CP were used for the validation of the shape reconstruction. The femoral anteversion angle of the test subjects ranged from 7–61°, with a mean of 31° and standard deviation of 15° The mean error was 2.03 mm (SD 0.60 mm, 95% CI 1.79–2.27 mm) by the means of PS-RMS. The mean PS-RMS error was 1.84 mm (SD 0.32 mm, 95% CI 1.74–1.95 mm) using a known calibration environment with DRR. The mean PS-RMS error was 1.93 mm (SD 0.43 mm, 95% CI 1.79–2.06 mm) when the calibration process was involved with DRR (Table 2).

Fig. 5 shows a surface heat map of the SSM to demonstrate where the maximum reconstruction errors occur. The maximum of 24 distances between the SSM and ground-truth shape for each vertex is indicated by a color scale, where blue indicates a 0-mm error and red indicates a 10-mm error. The mean Hausdorff distance from the SSM to ground-truth shape was 4.85 mm (SD 1.35 mm, 95% CI 4.30–5.39 mm).

4. Discussion

Using our newly developed protocol, the femur was successfully reconstructed in 3D by performing simultaneous calibration and shape optimization processes. The mean error of reconstruction, determined by means of the Hausdorff distance from the SSM to the ground-truth shape, was approximately 5 mm.

Our study has some limitations that should be addressed. First, our method was designed to perform femur reconstruction, which uses a smooth contour instead of sharp anatomical landmarks. The femur is a single bone, and further studies for bones comprising multiple parts, such as the foot or tibia, are required. Second, the segmentation algorithm uses a canny-edge detector; however, for blurry images and overlapped regions, the detector often fails. For femur segmentation, our algorithm worked well for recovering undetected edge points. However, for more complex and overlapping bones like the pelvis or foot, further refinement may be required.

The use of 3D reconstruction from un-calibrated 2D images has been reported in the field of computer vision. Azevedo et al. [21] described methods based on feature point matching. However, these methods require multiple views and good feature point matching for 3D reconstruction, and are hence not suitable for limited views of radiography and for smooth-shaped bones. Reconstructing 3D shapes of smooth bones from only two 2D radiographic images has no unique intrinsic solution. For example,

Please cite this article as: K. Youn et al., Iterative approach for 3D reconstruction of the femur from un-calibrated 2D radiographic images, Medical Engineering and Physics (2017), http://dx.doi.org/10.1016/j.medengphy.2017.08.016

Table 1
Rotation angle errors when digitally reconstructed radiograph images are calibrated using the ground-truth shape and statistical shape model compared to the Euler angles of ground-truth orientation.

Rotation axis	View + Shape	Mean	Standard deviation	95% CI	Maximum
Y	AP + GT	1.67	1.09	1.32 ~ 2.03	4.00
	AP + SSM	2.74	2.03	2.08 ~ 3.40	7.82
	LAT + GT	1.33	1.08	0.99 ~ 1.68	3.66
	LAT + SSM	2.29	1.69	1.74 ~ 2.83	5.46
X	AP + GT	3.15	2.47	2.35 ~ 3.95	8.98
	AP + SSM	4.30	3.24	3.25 ~ 5.34	11.82
	LAT + GT	4.32	2.91	3.38 ~ 5.26	13.00
	LAT + SSM	4.74	3.63	3.57 ~ 5.91	11.91

The data are presented as the number of degrees (°).
Abbreviations: CI, confidence interval; AP, anterior–posterior; GT, ground-truth; SSM, statistical shape model; LAT, lateral.

Table 2
Effects of calibration and shape optimization on the shape reconstruction error.

Test set	Mean	Standard deviation	95% CI	Maximum
Clinical radiographs + calibration + shape optimization	2.03	0.60	1.79~2.27	4.14
DRR + shape optimization	1.84	0.32	1.74~1.95	2.98
DRR + calibration + shape optimization	1.93	0.43	1.79~2.06	3.34

The data are presented in mm.
Abbreviations: CI, confidence interval; DRR, digitally reconstructed radiographs.

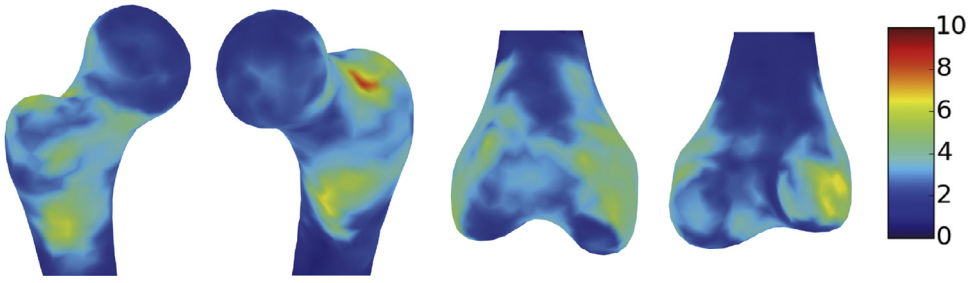

Fig. 5. A heat map depicting maximum errors of 24 reconstructions. Blue indicates a 0-mm error and red indicates a 10-mm error. (For interpretation of the references to color in this figure legend, the reader is referred to the web version of this article.)

the 2D projection of a cylinder and cube appear as identical rectangles in the AP and LAT views. Therefore, prior knowledge of 3D shapes in terms of whether the 2D rectangle comes from a cylinder or cube can help resolve this ambiguity. Furthermore, if the possible variations of a 3D shape are known, we can select a unique solution matching the image; The SSM contains a mean vector and most variant shape offset vectors, which represent the training dataset. The statistical model is useful for expressing the shape variations that it is built from, but does not provide useful information about the shapes not included in the training data. Chaibi et al. [5] proposed an SSM for normal subjects, and this SSM will hence work for most normal individuals. However, on the other hand, patients with CP have a very large variance in the femoral anteversion and coxa valga compared to normal subjects. In the present study, we built our SSM using the femurs of 54 CP patients. Therefore, our method is expected to be more accurate than those of other studies for 3D femur reconstruction of the femur in CP patients. The maximum errors identified by the heat map (Fig. 5) were the highest in the greater trochanter, lesser trochanter, and medial distal condyle. However, the effects of such errors on clinical measurements, such as of the femoral anteversion and neck shaft angle, are considered to be tolerable.

Three-dimensional reconstruction is the process of obtaining a shape that matches the 2D images when it is projected onto AP and LAT views. Therefore, locating the positions where the bi-planar radiographic images are obtained is important. This process is called calibration. The easiest way to obtain calibrated radiographic images is by fixing two radiographic systems and acquiring bi-planar images simultaneously, which is known as a pre-calibrated system. For example, the pre-calibrated EOS® system comprises two orthogonally fixed X-ray imaging devices and acquires two orthogonal head-to-feet calibrated X-ray images simultaneously, with the patient in a weight-bearing standing pose [3]. However, this system requires a large installation space and additional expensive apparatus. Purchasing an EOS® system only for 3D reconstruction may hence not be appropriate in some hospitals or countries. In cases where using a pre-calibrated system is not feasible, algorithms that perform post-calibration using metal markers have been proposed. The earlier approaches used direct linear transformation, which requires a rigid object with attached metal markers whose 3D positions are known [22]. André et al. [23] proposed spine reconstruction based on such direct linear transformation calibration. Subsequently, explicit calibration was proposed, allowing the positions of the metal makers to remain unknown. Explicit calibration optimizes the calibration parameters so that

Please cite this article as: K. Youn et al., Iterative approach for 3D reconstruction of the femur from un-calibrated 2D radiographic images, Medical Engineering and Physics (2017), http://dx.doi.org/10.1016/j.medengphy.2017.08.016

the estimated metal marker position from their stereo points on images fit to those points when re-projected onto the images. Cheriet et al. [8] proposed spine and rib cage reconstruction using explicit calibration. Because the positioning of large objects is cumbersome, Moura et al. [24] and Kadoury et al. [15] proposed a small calibration object to minimize the impact of the calibration object. However, positioning a small object with metal makers still restricts its practical use, because this usually requires modification to the existing clinical routine. Therefore, studies calibrating without the use of metal markers have been performed. Kadoury et al. [16] proposed self-calibration, which uses anatomical landmarks instead of metal markers, for explicit calibration and showed that using the vertebrae as landmarks can be used as an alternative to metal markers for spine reconstruction, with no significant increase in error. The reason this approach works is that each vertebra has plenty of sharp landmark points that can be identified on both AP and LAT views. However, self-calibration is not applicable to the femur, because it has a smooth surface and there are thus no landmarks that can be identified on both views.

The parameters of radiographic system calibration consist of 1) the X-ray source to image-receptor distance (SID); 2) the 2D coordinate of the X-ray source when it is orthogonally projected onto an image, called the principal point; and 3) the orientation and position of the image plane in the object reference frame (equivalently, the orientation and position of the object in the image reference frame). Moura et al. [25] described the radiographic calibration parameters in detail. These parameters form a view of the radiographic system, and we use the terms 'view' and 'orientation and position of the image plane' interchangeably when the SID and principal point are known. Herein, we observed that the SID and principal point can be determined without calibration using conventional radiographic systems. In practice, the radiologic technologist aims the X-ray source tube at the center of the detection plane, which moves the principle points to the center. The SID is usually fixed according to the clinical routines, and some digital radiograph devices record and save these parameters automatically. Hence, we only need to estimate the third parameter to obtain calibrated radiographic images for conventional systems. Estimating the third parameter, assuming the others are known, is called a pose-estimation problem. The PnP method is an efficient algorithm for solving pose-estimation based on known 3D points and their 2D projection on images. The PnP method determines the view so that the 3D points matches their 2D coordinates when they are projected onto an image from a given view. Zheng and Zhang [26] proposed to use PnP for estimating the pose of the pelvis by matching the landmarks of their SSM to the landmarks of 2D images. However, as mentioned above, the femur has no such landmarks. The PnP method is also used in other areas such as augmented reality for positioning 3D objects on an image [27] and for manipulating 2D images of a 3D object [28]. However, the work relies on known 3D objects, and without this, accurate calibration is difficult. In other words, we need an exact 3D model to obtain accurate orientation and position of the image. However, to achieve this, accurate orientation and position of the image are first required. Thus, these two problems become dependent and have to be solved jointly. Our contribution is pose estimating from these uncertainties using the contours of an SSM and images.

The prerequisite of contour-based pose-estimation is a contour segmentation. There are many segmentation methods for photographs. However, projective radiographic images are associated with different characteristics and segmentation difficulties compared to photographic images. First, transparency results in overlapped boundaries of the bones. Second, the intensity varies proportionally to the thickness, thus showing smooth gradations at boundaries. Photographic segmentation methods, which use only pixel intensities, fail to catch the overlapped and blurred boundaries on medical images. Accordingly, segmentation methods for projective radiographic images often utilize a-priori knowledge of the region of interest. Lindner et al. [29] used random forest regression trained from manually labeled proximal femur images for segmentation. Dong and Zheng [30] segmented the proximal femur contour using a pose-estimated 3D SSM. Xie et al. [31] segmented the proximal femur by fitting a 2D SSM built from manually segmented radiographs. However, their work concentrated on proximal femur segmentation and did not address the diverse pose of the entire shape. Recently, deep learning medical image analysis has attracted more attention, with Cernazanu-Glavan and Holban [32] proposing a convolution neural network for bone segmentation. However, deep learning requires a lot of training data for its performance, and obtaining the ground-truth training data is time-consuming and currently unavailable.

The radiographs of patients with CP are often not standardized because these patients cannot pose like normal subjects, owing to muscle contracture, spasticity, and bony deformities. Osteoporosis is also common in CP, resulting in the bones appearing blurry on imaging. Therefore, we used a pose-estimated 3D SSM as the reference contour to deal with the various poses of CP patients in the present study. For undetected points due to blurred images, we can predict their existence by drawing all possible lines between the detected points. However, this would be intractable, and we thus used Delaunay triangulation to connect the closest edge points while taking care not to overlap the other prediction lines. Originally, Delaunay triangulation was described as a method for dividing images into triangles so that the minimum angle of the triangles would be maximized [33]. In our work, Delaunay triangulation was used to keep the number of prediction lines within a reasonable range. To resolve the issue of overlapping boundaries, we constrained the extracted contour to pass six user-inputted points while aligning well with the reference contour, because the six points are guaranteed to be on the contour by the user. This approach worked for the femur and segmented contours successfully.

The contour-based pose estimation is a process of searching the view so that the contour projection of the shape fits with the segmented contour of the image. The contour of the 3D femur and its correspondence to the image contour change as the view changes; thus, we cannot use the PnP method directly, because it assumes fixed 3D–2D correspondences. Herein, we first updated the view using the iterative PnP method [19], assuming that the contour in the current view is fixed. Subsequently, we updated the contour and its correspondence from the given view. These steps are iteratively performed until convergence. Generally, the accuracy of iterative approaches depends on the initial condition because of the process may fall into local optima. We speculated that the initial orientation of the view has an impact on the accuracy. We evaluated calibration errors as factors of the AP and LAT viewing directions, and viewing angles along the X and Y axes (Table 1). We observed that the angles along the X axis were calibrated less accurately than those along the Y axis. Adjusting the angles along the Y axis can correct the mismatch associated with the femur head and distal condyles, while the angles along the X axis aligns the shaft of the femur. That explains why the calibration errors along the X axis are larger than the errors along the Y axis. We also observed that the largest errors occurred in LAT views, which were used to generate DRRs with the patient's posture midway between the lateral recumbent and prone positions. We found that our method works better if the patient's femur is positioned in a way such that it is not inclined to X-ray detection plane and the patient's posture is midway between the lateral recumbent and supine positions. Since some patients with CP cannot assume the standard

Please cite this article as: K. Youn et al., Iterative approach for 3D reconstruction of the femur from un-calibrated 2D radiographic images, Medical Engineering and Physics (2017), http://dx.doi.org/10.1016/j.medengphy.2017.08.016

supine position, further improvement is required with respect to the X-angle pose estimation.

Our iterative approach can be summarized as computing the best value for the calibration parameters given a shape and subsequently using the computed calibration values to optimize the shape iteratively. We formulated shape optimization as a least square fitting problem and solved it analytically. The calibration was solved based on contour by updating the view and the correspondence between the contours simultaneously using the iterative PnP method. Shape reconstruction from uncalibrated radiographs inherently involves such nonlinear functional components as deforming and fitting 3D shape meshes to 2D contours and perspective projection for viewing transformation. Handling of the non-linear functions is the key to the successful reconstruction and fast computation. Our method separates nonlinear effects, caused by the iterative refinement of parameters, from the linear part to allow for least square fitting. This separation achieved not only an order of magnitude speedup but improvements in reconstruction accuracy.

In conclusion, in this study, we proposed a method to reconstruct the 3D femur shape from un-calibrated bi-planar radiographic images. This method can be applied without disturbing the existing clinical routine and without the need for large or costly devices.

Acknowledgement

This research was supported by the MSIT (Ministry of Science and ICT), Korea, under the SW Starlab support program (IITP-2017-0536-20170040) supervised by the IITP (Institute for Information & communications Technology Promotion). This research was supported by Basic Science Research Program through the National Research Foundation of Korea (NRF) funded by the Ministry of Science, ICT & Future Planning (No. NRF- 2017R1A2B4007412).

References

[1] Chung CY, Lee KM, Park MS, Lee SH, Choi IH, Cho T-J. Validity and reliability of measuring femoral anteversion and neck-shaft angle in patients with cerebral palsy. JBJS 2010;92:1195–205.
[2] Pirpiris M, Trivett A, Baker R, Rodda J, Nattrass G, Graham H. Femoral derotation osteotomy in spastic diplegia. Bone & Joint Journal 2003;85:265–72.
[3] EOS imaging n.d. http://www.eos-imaging.com/ (accessed April 4, 2017).
[4] Dubousset J, Charpak G, Dorion I, Skalli W, Lavaste F, Deguise J, et al. A new 2D and 3D imaging approach to musculoskeletal physiology and pathology with low-dose radiation and the standing position: the EOS system. Bulletin de l'Académie nationale de médecine 2005;189:287–97; discussion 97-300.
[5] Chaibi Y, Cresson T, Aubert B, Hausselle J, Neyret P, Hauger O, et al. Fast 3D reconstruction of the lower limb using a parametric model and statistical inferences and clinical measurements calculation from biplanar X-rays. Computer methods in biomechanics and biomedical engineering 2012;15:457–66.
[6] Faria R, McKenna C, Wade R, Yang H, Woolacott N, Sculpher M. The EOS 2D/3D X-ray imaging system: a cost-effectiveness analysis quantifying the health benefits from reduced radiation exposure. European journal of radiology 2013;82:e342–9.
[7] Mitton D, Landry C, Veron S, Skalli W, Lavaste F, De Guise JA. 3D reconstruction method from biplanar radiography using non-stereocorresponding points and elastic deformable meshes. Medical and Biological Engineering and Computing 2000;38:133–9.
[8] Cheriet F, Laporte C, Kadoury S, Labelle H, Dansereau J. A novel system for the 3-D reconstruction of the human spine and rib cage from biplanar X-ray images. IEEE transactions on biomedical engineering 2007;54:1356–8.
[9] Zheng G, Schumann S. 3-D reconstruction of a surface model of the proximal femur from digital biplanar radiographs. Engineering in Medicine and Biology Society, 2008 EMBS 2008 30th Annual International Conference of the IEEE: IEEE 2008:66–9.
[10] Valstar ER, Gill R, Ryd L, Flivik G, Börlin N, Kärrholm J. Guidelines for standardization of radiostereometry (RSA) of implants. Acta orthopaedica 2005;76:563–72.
[11] Kurazume R, Nakamura K, Okada T, Sato Y, Sugano N, Koyama T, et al. 3D reconstruction of a femoral shape using a parametric model and two 2D fluoroscopic images. Computer Vision and Image Understanding 2009;113:202–11.
[12] Dworzak J, Lamecker H, von Berg J, Klinder T, Lorenz C, Kainmüller D, et al. 3D reconstruction of the human rib cage from 2D projection images using a statistical shape model. International journal of computer assisted radiology and surgery 2010;5:111–24.
[13] Laporte S, Skalli W, De Guise J, Lavaste F, Mitton D. A biplanar reconstruction method based on 2D and 3D contours: application to the distal femur. Computer Methods in Biomechanics & Biomedical Engineering 2003;6:1–6.
[14] Baka N, Kaptein BL, de Bruijne M, van Walsum T, Giphart JE, Niessen WJ, et al. 2D–3D shape reconstruction of the distal femur from stereo X-ray imaging using statistical shape models. Med Image Anal 2011;15:840–50. doi:10.1016/j.media.2011.04.001.
[15] Kadoury S, Cheriet F, Laporte C, Labelle H. A versatile 3D reconstruction system of the spine and pelvis for clinical assessment of spinal deformities. Medical & biological engineering & computing 2007;45:591–602.
[16] Kadoury S, Cheriet F, Labelle H. Self-calibration of biplanar radiographic images through geometric spine shape descriptors. IEEE transactions on biomedical engineering 2010;57:1663–75.
[17] Park N, Lee J, Sung KH, Park MS, Koo S. Design and validation of automated femoral bone morphology measurements in cerebral palsy. Journal of digital imaging 2014;27:262–9.
[18] Ferrarini L, Olofsen H, Palm W, Vanbuchem M, Reiber J, Admiraalbehloul F. GAMEs: growing and adaptive meshes for fully automatic shape modeling and analysis. Med Image Anal 2007;11:302–14. doi:10.1016/j.media.2007.03.006.
[19] Lu CP, Hager GD, Mjolsness E. Fast and globally convergent pose estimation from video images. IEEE T Pattern Anal. 2000;22:610–22.
[20] 3D Medical Image Processing Software | Materialise Mimics n.d. http://www.materialise.com/en/medical/software/mimics (accessed April 4, 2017).
[21] Azevedo TCS, Tavares JMRS, Vaz MAP. 3D Object reconstruction from uncalibrated images using an off-the-shelf camera. Advances in computational vision and medical image processing. Netherlands: Dordrecht: Springer; 2009. p. 117–36. doi:101007/978-1-4020-9086-8_7.
[22] Abdel-Aziz Y, Karara HM, Hauck M. Direct linear transformation from comparator coordinates into object space coordinates in close-range photogrammetry. Photogramm Eng Remote Sens 2015;81:103–7. doi:10.14358/PERS.81.2.103.
[23] André B, Dansereau J, Labelle H. Optimized vertical stereo base radiographic setup for the clinical three-dimensional reconstruction of the human spine. J Biomech 1994;27:1023–35. doi:10.1016/0021-9290(94)90219-4.
[24] Moura DC, Barbosa JG, Tavares JMRS, Reis AM. Calibration of bi-planar radiography with a rangefinder and a small calibration object. Berlin, Heidelberg: Springer; 2008. p. 572–81. doi:10.1007/978-3-540-89639-5_55.
[25] Moura DC, Barbosa JG, Reis AM, Manuel J, Tavares RS. A flexible approach for the calibration of biplanar radiography of the spine on conventional radiological systems. Comput Model Eng Sci 2010;60:115–38. doi:10.3970/CMES.2010.060.115.
[26] Zheng G, Zhang X. Computer assisted determination of acetabular cup orientation using 2D–3D image registration. Int J Comput Assist Radiol Surg 2010;5:437–47. doi:10.1007/s11548-010-0407-x.
[27] Crivellaro A, Lepetit V. Robust 3D tracking with descriptor fields. In: Proceedings of the IEEE Conference on Computer Vision and Pattern Recognition; 2014. p. 3414–21.
[28] Kholgade N, Simon T, Efros A, Sheikh Y. 3D object manipulation in a single photograph using stock 3D models. ACM Transactions on Graphics (TOG) 2014;33:127.
[29] Lindner C, Thiagarajah S, Wilkinson J, Consortium T, Wallis G, Cootes T. Fully automatic segmentation of the proximal femur using random forest regression voting. IEEE transactions on medical imaging 2013;32:1462–72.
[30] Dong X, Zheng G. Automatic extraction of proximal femur contours from calibrated X-ray images using 3D statistical models. International Workshop on Medical Imaging and Virtual Reality: Springer 2008:421–9.
[31] Xie W, Franke J, Chen C, Grützner PA, Schumann S, Nolte L-P, et al. Statistical model-based segmentation of the proximal femur in digital antero-posterior (AP) pelvic radiographs. International journal of computer assisted radiology and surgery 2014;9:165–76.
[32] Cernazanu-Glavan C, Holban S. Segmentation of bone structure in X-ray images using convolutional neural network. Adv Electr Comput Eng 2013;13:87–94.
[33] Aurenhammer F, Klein R, Lee D-T. Voronoi diagrams and delaunay triangulations. World Scientific; 2013. doi:10.1142/8685.